Electronic Supplementary file

Synergistic Effect of Acid-Etched g-C_3N_4 Nanosheets and Polyaniline Nanofibers for the Adsorption and Photocatalytic Degradation of Textile Dyes: Study of Charge Transfer Mechanism and Intermediate Products

Arun Kumar[1], Honey Mittal[1] Rupali Nagar[2] and Manika Khanuja[1*]

[1]Centre for Nanoscience and Nanotechnology, Jamia Millia Islamia, New Delhi - 110025, India

[2]Nanomaterials for Energy Applications Lab, Applied Science Department, Symbiosis Institute of Technology, Symbiosis International (Deemed University), Lavale, Pune-412115, Maharashtra, India

**Corresponding author manikakhanuja@gmail.com*

1. Experimental

1.1 Materials

Melamine ($C_3H_6N_6$) was purchased from Mumbai, India (Loba Chemie Pvt. Ltd.). Methyl Orange ($C_{14}H_{14}N_3NaO_3S$), Hydrogen peroxide (H_2O_2), Hydrochloric acid (HCl, 99.96%) and Sulphuric acid (H_2SO_4) were purchased from Mumbai, India (Thermo Fisher Scientific Pvt. Ltd.). Aniline ($C_6H_5NH_2$, 99.98%), Congo Red ($C_{32}H_{22}N_6Na_2O_6S_2$) and *tert*-butyl alcohol ($(CH_3)_3COH$) were used from New Delhi, India (Central Drug House(P) Ltd.). Potassium iodide (KI) was purchased from Pallav Chemicals and Solvents Pvt. Ltd., Mumbai, India. Benzoquinone ($C_6H_4O_2$) was purchased from Molychem Pvt. Ltd., Mumbai, India. Ammonium persulfate ($(NH_4)_2S_2O_8$) with 0.0005% (max impurity limits) was purchased from Sisco Research Pvt. Ltd., New Delhi, India.

1.2 Synthesis of acid-etched g-C_3N_4 (TGCN)

The facile synthesis of g-C_3N_4 (GCN) was performed using thermal condensation method. To synthesize GCN, fine melamine powder (5 g) was taken in the crucible and kept the crucible at 550 ºC in the muffle furnace for 3 hours at 5 ºC /min ramp rate. The obtained yellow material was bulk GCN. For the synthesis of TGCN, 40 ml solution consist of H_2SO_4 and HNO_3 in 1:1 ratio was prepared and, 2 g of the bulk GCN was added in it. The solution was performed under ultrasonication for 3 hours. The obtained solution was also performed to centrifuge for 10 min at 10,000 rpm and then collected after sequentially washing with acetone and DI water to separate impurity. The final product was dried at 80 °C for 12 hours[1].

1.3 Characterization

Field emission scanning electron microscope (FESEM) was used to observe the surface morphology of the prepared samples using Quanta 3D FEG (FEI's). The structural and crystalline properties of the prepared samples was analyzed with the help of X-ray diffraction (XRD) technique using Rigaku Smart Lab (2θ Range: 5° to 40°). The Fourier transform of infrared (FTIR) spectroscopy and Raman spectra were recorded from Bruker Tensor 37 in between the range of 500-4000 cm^{-1}. The study of absorbance spectrum of the prepared photocatalysts were investigated using UV-Vis spectrometer from Agilent technologies, Cary 100 series.

1.4 Adsorption and photocatalytic degradation experiment

To evaluate the performance of TGCN and TCP (TCP30, TCP50 and TCP80) nanocomposites, adsorption and photocatalytic degradation of Methyl orange (MO) and Congo red (CR) were studied. The dye removal efficiency and pseudo-first order kinetics were also identified.

$$efficiency\ (\eta) = \left(1 - \frac{C_t}{C_o}\right) * 100 \qquad \text{(S1)}$$

$$q_t = \frac{(C_o - C_t)V}{m} \quad \text{(S2)}$$

$$ln(q_e - q_t) = ln\, q_e - k_1 t \quad \text{(S3)}$$

$$-\ln\left(\frac{C_t}{C_o}\right) = k_2 t \quad \text{(S4)}$$

The adsorption and photocatalytic degradation efficiency of MO and CR were evaluated using the Eq. S1, Where C_o (mg/L) stands for the dye concentration at t = 0, C_t (mg/L) denotes dye concentration at time t. V (L) is the volume of the dye solution used in the experiment and m (mg) is the mass of the synthesized material. The pseudo-first order kinetics of adsorption and photocatalytic degradation of MO and CR using TGCN and TCP nanocomposites were studied using Eq. S2 and S3. Where q_e (mg/g) and q_t (mg/g) denotes for the amount adsorbed dye at equilibrium reached and at time t, respectively, k_1 (min^{-1}) and k_2 (min^{-1}) are the rate constant of pseudo-first order adsorption and photocatalytic degradation process. The 'k' values were evaluated using the slopes obtained from the linear fitting as shown in Fig. 2(c) and 2(d).

Table S1: Previous reports of g-C_3N_4 based nanomaterials for the photocatalytic degradation of different dyes

Material	Synthesis method	Morphology	Pollutant	Pollutant removal rate	References
TGCN/PANI (TCP50)	In-situ polymerization method	Nanosheets with nanofibers	MO CR	99.3 % in 25 min 99.0 % in 150 min	This work
g-C_3N_4/TiO_2@Polyaniline	Lamellar structure of TiO2 with PANI on the surface	In-situ oxidative polymerization methods	CR	100 % in 180 min	[2]

$g\text{-}C_3N_4$	microrods	Chemical method	MO	100 % in 140 min	[3]
$g\text{-}C_3N_4$/RGO/BFO	Hydrothermal method	Porous structure	CR	87.7 % in 60 min	[4]
0.2 wt % Co_3O_4-g-C_3N_4	Mixing and heating method	Agglomerated crystal structure	CR	100 % in 180 min	[5]
PANI/$g\text{-}C_3N_4$	In-situ oxidative polymerization	Aggregated particles	MO	92.8% in 120 min	[6]
7 wt % PANI/BiOCl	Plate like structure with small particle	Chemisorptions method	MO	67 % in 210 min	[7]
PANI-TiO_2	Porous structure	Assembly method	MO	98.1% in 6 h	[8]
PANI/MWCNT-APS	Microemulsion polymerization method	Fibre-like	CR	91%	[9]
TMC-incorporated Carbon Nitride	Chemical condensation	hexagonal and quadrangle honeycomb-like	MO	60% in 120 min	[10]

		structure			
PANI–SWCNT	In situ chemical polymerization technique	Little agglomerated PANI over SWCNT	MO	94.35 % in 30 min	[11]

2. Results and discussion

The FESEM images of TGCN (Fig. S1a and S1b) shows a solid agglomeration of sheet-like morphology to several micrometres, indicated the formation of tri-s-triazine rings[12]. The FESEM images of PANI doped TGCN nanocomposites viz. TCP30, TCP50, and TCP80 are shown in Fig S1(c, e, &g). After the polymerization, nanofibers of PANI were occupied on the surface of TGCN and a combined morphology of both fibrous and layered structure were obtained. TCP nanocomposites (TCP30, TCP50, and TCP80) exhibited lesser diameter and denser interlinked states between TGCN and PANI than pristine TGCN. Fig. S1(d, f, &h) represents the FESEM images of TCP30, TCP50 and TCP80 nanocomposite. The nanofibers of PANI presents on the surface of TGCN formed the synergistic interface between PANI and TGCN. Fig. S2(a) showed the XRD plot of TCP (TCP30, TCP50 and TCP80) nanocomposites. The pristine TGCN can be identified with two clear XRD peaks at 12.68º and 27.34º, which corresponds to (100) and (002) peaks of JCPDS 87-1526. The two characteristic peaks are found in good agreement with the standard reported data[1]. The XRD peak position corresponding to PANI was observed at 2θ = 14.4º, 20.46º and 24.88º belongs to the (hkl) planes of (011), (020) and (200), which confirmed the formation of PANI[13, 14]. In the XRD spectra of TCP nanocomposites, a minor peak at 27.34º was ascribed to (002) plane indicated

the presence of TGCN nanosheets. Besides, other XRD peaks of nanofibrous PANI were detected simultaneously, indicating the presence of TGCN nanosheets and PANI nanofibers. The XRD results are also in good agreement with HR-TEM SAED patterns.

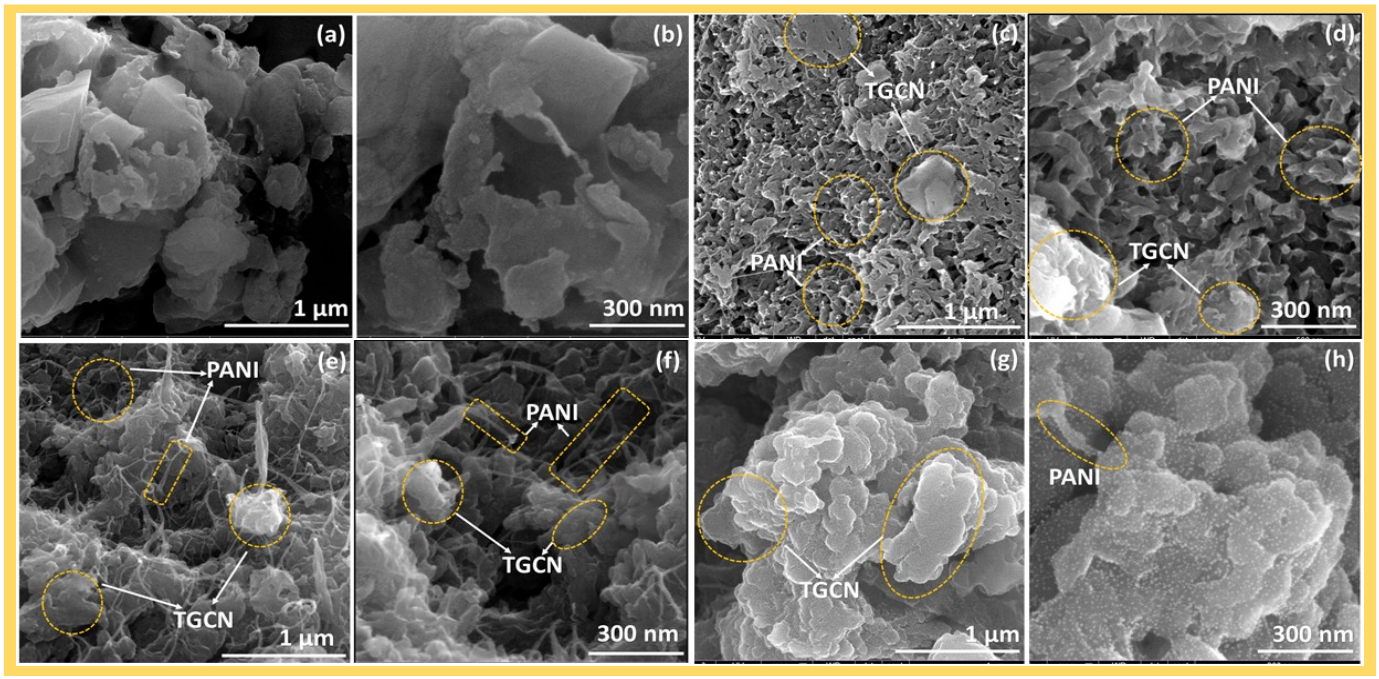

Fig. S1. FESEM images of (a, b) TGCN (c, d) TCP30 (e, f) TCP50 and (g, h) TCP80.

The FTIR spectra of TGCN, PANI and TCP nanocomposites are shown in Fig. S2(b). The observed FTIR peaks position appeared at 795 cm^{-1} (PANI) corresponds to heptazine units, indicating the identification of TGCN. The FTIR bands observed at 1062 and 1556 cm^{-1} represented the OH and CO functional groups which were responsible for the creation of oxygen containing functional groups[12]. The FTIR bands in the region from 1253 to 1409 cm^{-1} and 1643 cm^{-1} were attributed to the C-N and C=N stretching vibrations[15, 16]. The characteristic FTIR peaks observed at 1490 and 1586 cm^{-1} are due to C=C and C-N stretching vibrations of the benzenoid and quinoid rings, respectively[17]. The FTIR peaks at 2368 and 3743 cm^{-1}

appeared due to physically adsorbed CO_2 and H_2O from the atmosphere[16]. The broad peak at 3040 cm^{-1} was assigned to CO_2, primary and secondary vibrational stretching[1]. The FTIR bands of other nanocomposites (TCP30 and TCP50) was almost in resembles to the pristine TGCN. However, some FTIR peaks were not seen in TCP80. This might be due to the high concentration of TGCN in TCP80 which reduced the effect of PANI. The FTIR results indicated the interaction between the TGCN and PANI had been formed and responsible for the good effect on the stability of the nanocomposite.

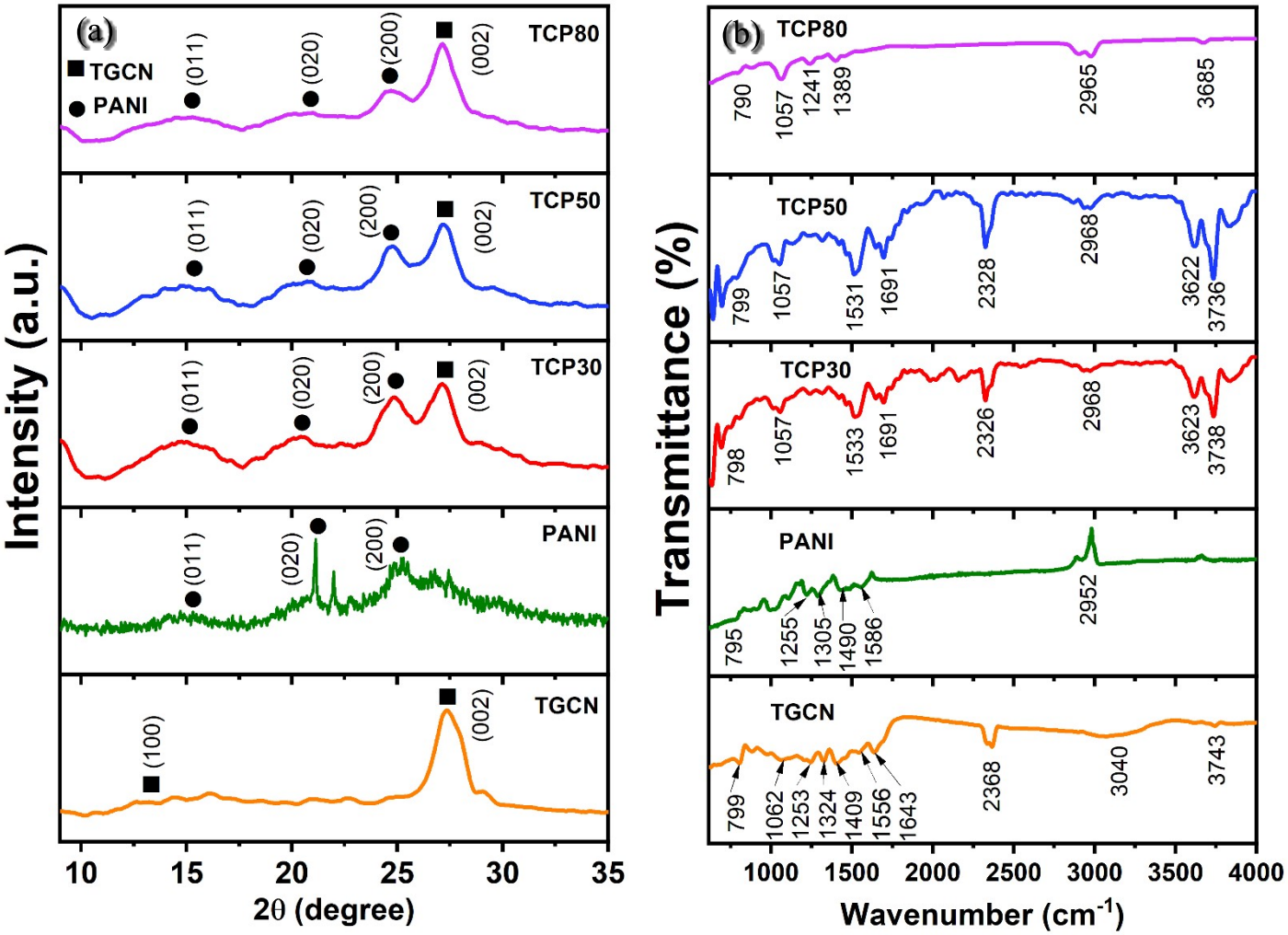

Fig. S2. (a) XRD and (b) FT-IR plots of TGCN, PANI, TCP30, TCP50 and TCP80.

The UV-Vis absorption spectra were used to study optical properties of prepared nanocomposites as shown in Fig. S3 (a-e). TGCN and PANI possessed indirect and direct optical band gaps. The energy band gap of TCP nanocomposites was determined assuming direct optical transitions as PANI was the base material. The bandgap (E_g) of all the synthesized samples were calculated from Tauc's plot using Eq. S5. The optical bandgap was calculated using Tauc's plot and results are shown in insets of Fig. S3 (a-e).

$$\alpha h\upsilon = (h\upsilon - E_g)^n \quad \text{(S5)}$$

where h is the Planck's constant, α is the absorption coefficient, ν is the frequency, E_g is the band width of the photocatalyst, n is the number that determines the transition property which is taken as 0.5 for direct bandgap and 2 for indirect bandgap semiconductor. The calculated optical bandgap of TGCN was found to be 2.65 eV which is suitable for visible light and follows the same with reported literature[1]. However, the optical bandgap of other prepared materials such as PANI, TCP30, TCP50 and TCP80 was found to be 2.72, 2.49, 2.68 and 2.74 eV which follow the higher significant values as TGCN concentration was increased from TCP30 to TCP50. The very close values of optical bandgap in TCP50 and TCP80 describes the stability of the value achieved compared to TCP30. The visible light driven bandgap of TCP nanocomposites makes it a suitable photocatalyst as compared with TGCN.

Fig. S3 (f) presents the Raman spectra for TCP30, TCP50 TCP80 nanocomposites. The absorption band at 1618 cm^{-1} and 1189 cm^{-1} describes the C-C bending vibration of benzenoid ring and C-H stretching vibration of semi-quinonoid ring[18]. The band at 876 cm^{-1}, 816 cm^{-1} , 507 cm^{-1} and 419 cm^{-1} are assigned with the in and out planar vibrations of protonated emeraldine rings of PANI[19]. The adsorption band at 976 cm^{-1} denoted the N-bending parallel modes of triazine units in TCP nanocomposite[20]. In order to study the defects and disorder in TGCN based nanocomposites viz., TCP30, TCP50 and TCP80, intensity ratio of D and G band (I_D/I_G) was very useful. The D band (1340 cm^{-1}) was identified with the defect states and G

(1482 cm^{-1}) band was associated with graphitic carbon. The evaluated I_D/I_G ratio of TCP30, TCP50 and TCP80 were 0.98, 0.99 and 0.98, respectively. The Raman spectroscopy confirmed the formation of TCP nanocomposites with more defeats on the surface of TCP50 as compared to other nanocomposites.

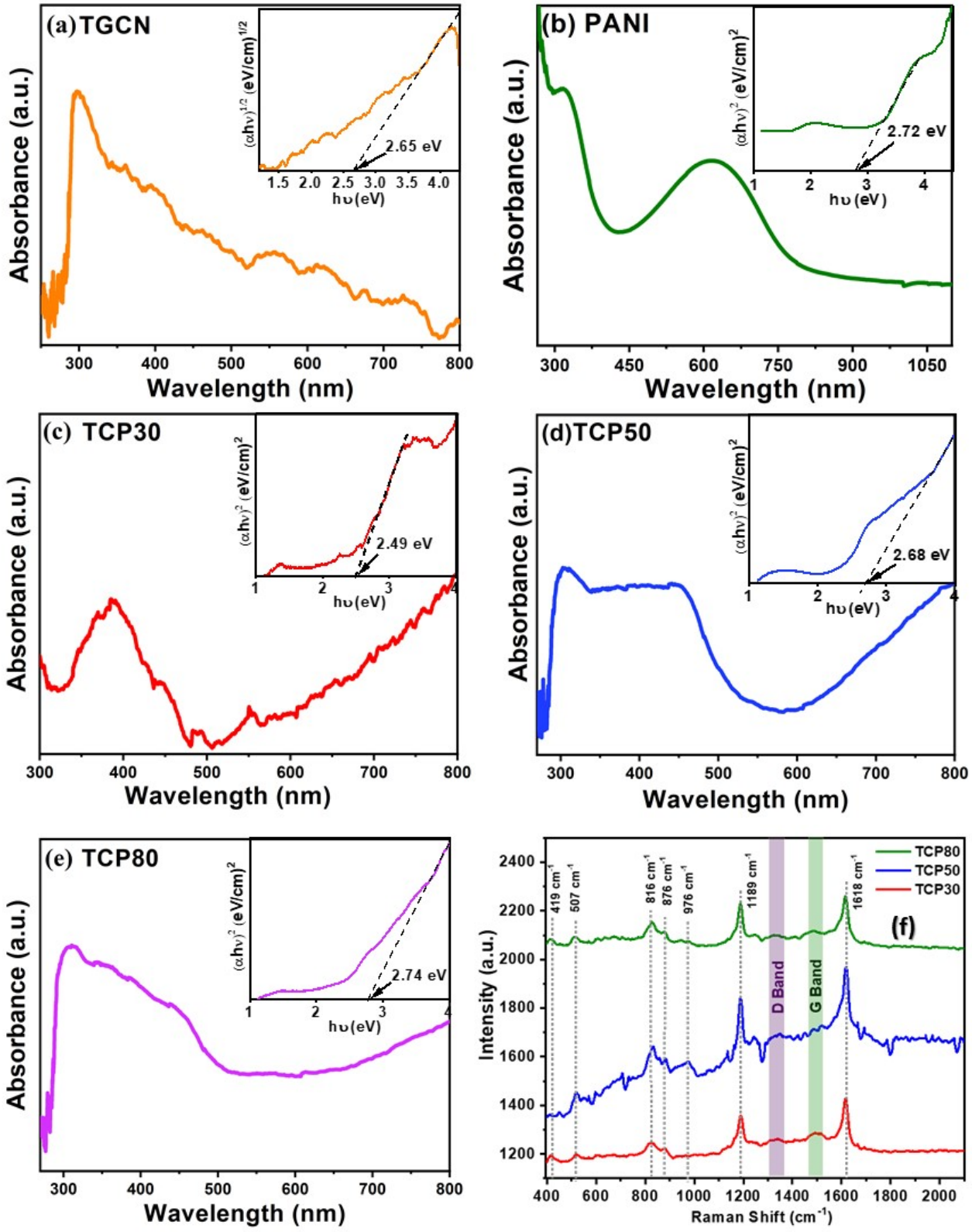

Fig. S3. UV-Vis absorption (inset: Tauc's plot) (a) TGCN, (b) PANI, (c) TCP30, (d) TCP50, (e) TCP80 and (f) Raman spectra of TCP30, TCP50 and TCP80.

Fig. S4 showed the N_2 adsorption-desorption isotherms of the prepared nanomaterials, TGCN, TCP30, TCP50 and TCP80. The obtained BET curves exhibit H3 hysteresis typical with type IV physisorption. The specific surface areas of TGCN, TCP30, TCP50 and TCP80 were found to be 17.05, 36.31, 48.31 and 71.64 $m^2\ g^{-1}$ respectively. The specific surface areas enhanced from 17.05 to 71.64 $m^2\ g^{-1}$ with an increase in TGCN/PANI ratio in the synthesized material, as mentioned in Table 1. Pore size distribution plots are shown in Fig. S4 inset through BJH (Barret-Joyner-Halenda) method. The obtained results showed that the increasing TGCN/PANI ratio enhanced the pore volume in TCP50 nanocomposite which enables it to interact with a greater number of dye molecules for the photocatalytic degradation. The result of Brunauer-Emmett-Teller (BET) N_2 adsorption-desorption measurements is consistent with that of TEM (Fig. 3(a)), that is, the introduction of PANI nanofibers over TGCN results in porous structure

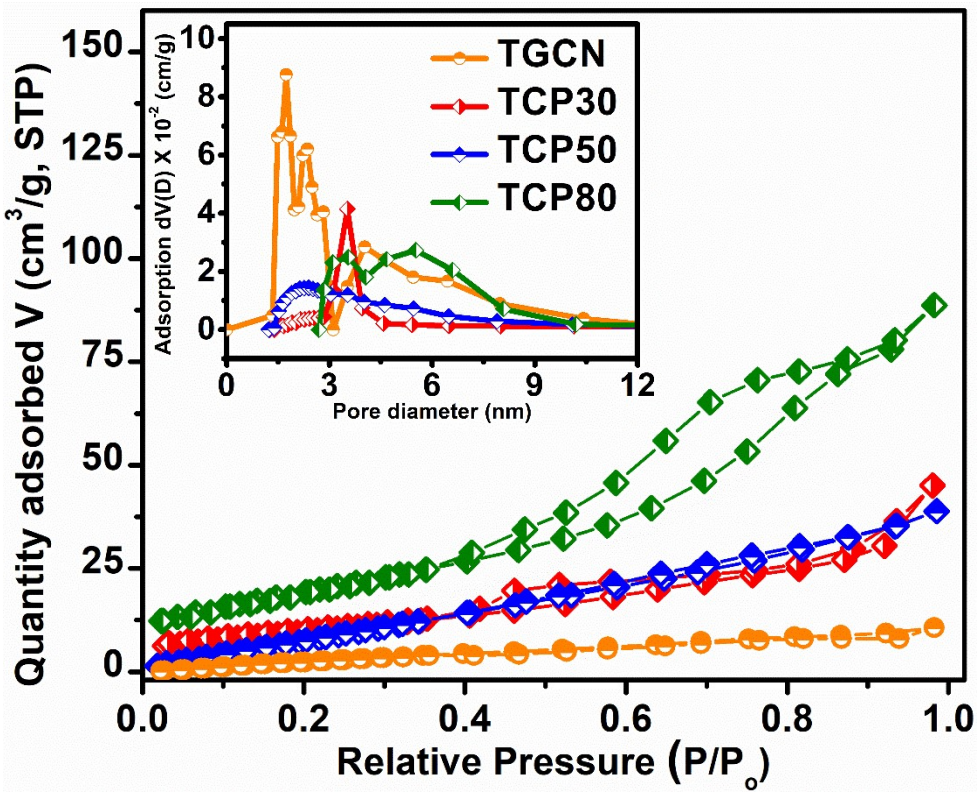

from TGCN to TCP80.

Fig S4. The BET N_2 adsorption-desorption curve of TGCN, TCP30, TCP50 and TCP80 with (inset) BJH plot of the distribution of pore size

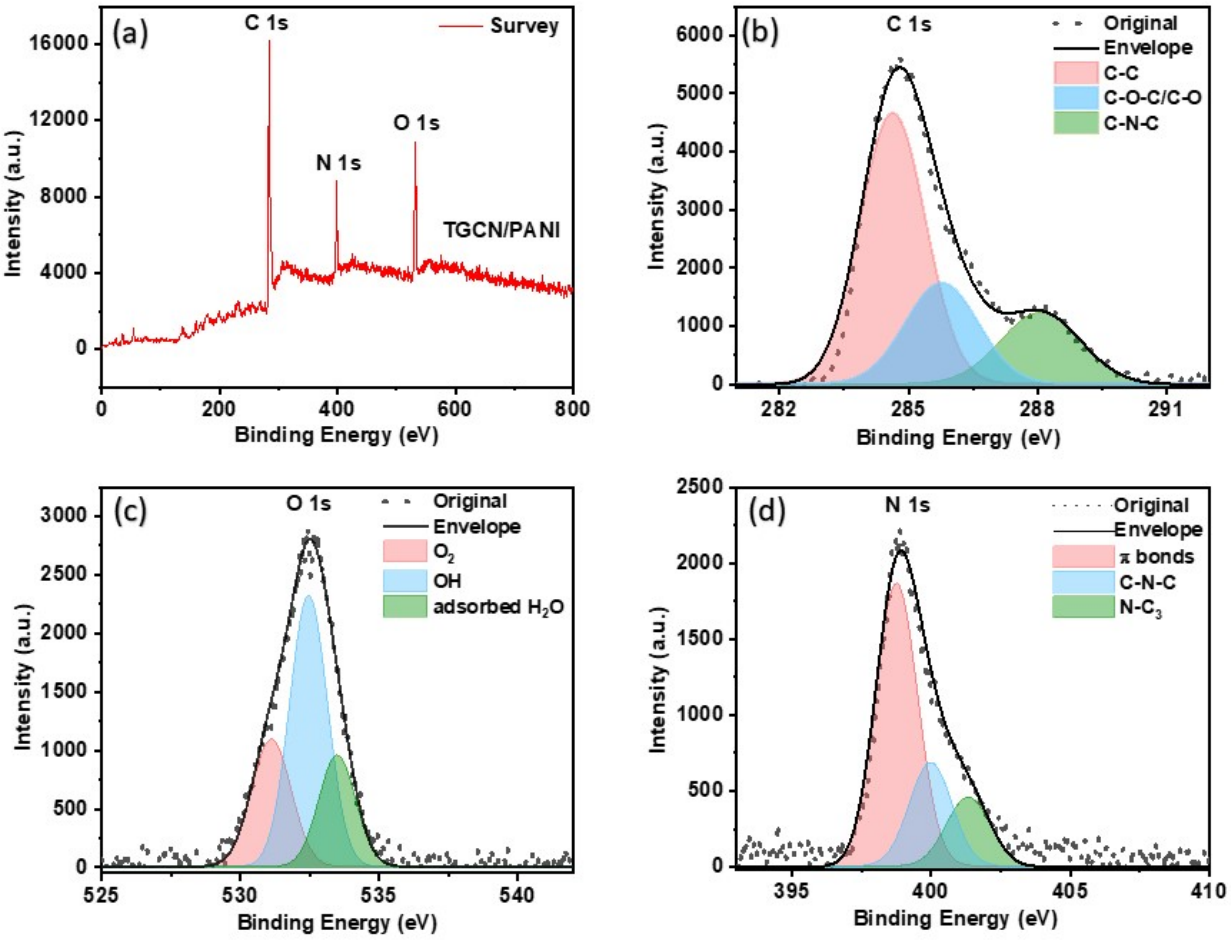

Fig. S5. (a) XPS survey spectra, (b) High-resolution C 1s, (c) O 1s, (d) N 1s XPS spectrum of TGCN/PANI (TCP50) nanocomposite.

X-ray photoelectron spectroscopy (XPS) was performed to study the chemical analysis of TGCN/PANI nanocomposite (TCP50). Fig. S5 Shows the general scan, and detailed elemental states of (b) C1s, (c) O1s and (d) N1s of TCP50, respectively. The deconvoluted C 1s spectrum containing three peaks located at 284.6, 286.7 and 288.1 eV, assigned to sp^2 hybridised C=C bond, carbon atoms of PANI or g-C_3N_4 atom linked to the nitrogen atom and the carbon atom that is bonded to nitrogen atoms, respectively[1]. N1s spectra of TCP50 nanocomposite can be

deconvoluted into three peaks located at 398.6, 400 and 401.3 eV, corresponded to π bonds in C=N, N-C_3 and C-N=C, respectively. The fitting of the deconvoluted O 1s spectra gives three peak centred at 531.2, 532.5 and 533.3 confirmed the presence of hydroxyl and carboxylic groups[1]. The slight shift in the peak positions is possibly due to the change in the electronic environment of elements in the TCP50 nanocomposite[20]

References

1. A. Kumar, S. Singh and M. Khanuja, Mater. Chem. Phys., 2020, **243**, 122402.
2. M. Alenizi, R. Kumar, M. Aslam, F. Alseroury and M. Barakat, Sci. Rep., 2019, **9**, 1-8.
3. I. Aslam, M. H. Farooq, U. Ghani, M. Rizwan, G. Nabi, W. Shahzad and R. Boddula, Mater. Sci. Technol., 2019, **2**, 401-407.
4. M. B. Shekardasht, M. H. Givianrad, P. Gharbani, Z. Mirjafary and A. Mehrizad, Diam. Relat. Mater., 2020, **109**, 108008.
5. C. Han, L. Ge, C. Chen, Y. Li, X. Xiao, Y. Zhang and L. Guo, Appl. Catal. B., 2014, **147**, 546-553.
6. L. Ge, C. Han and J. Liu, J. Mater. Chem., 2012, **22**, 11843-11850.
7. Q. Wang, J. Hui, J. Li, Y. Cai, S. Yin, F. Wang and B. Su, Appl. Surf. Sci., 2013, **283**, 577-583.
8. N. K. Jangid, S. Jadoun, A. Yadav, M. Srivastava and N. Kaur, Polym. Bull., 2021, **78**, 4743-4777.
9. R. S. Aliabadi and N. O. Mahmoodi, J. Clean. Prod., 2018, **179**, 235-245.
10. J. Wang, M. Li, M. Qian, S. Zhou, A. Xue, L. Zhang, Y. Zhao and W. Xing, Nanoscale Res. Lett., 2018, **13**, 248.
11. M. J. Chatterjee, A. Ghosh, A. Mondal and D. Banerjee, RSC adv., 2017, **7**, 36403-36415.
12. R. Kumar, M. Barakat and F. Alseroury, Sci. Rep., 2017, **7**, 1-11.
13. N. Parveen, N. Mahato, M. O. Ansari and M. H. Cho, Compos. B. Eng., 2016, **87**, 281-290.
14. S. H. Patil, A. P. Gaikwad, S. D. Sathaye and K. R. Patil, Electrochim. Acta, 2018, **265**, 556-568.
15. K. Pandiselvi, H. Fang, X. Huang, J. Wang, X. Xu and T. Li, J. Hazard. Mater., 2016, **314**, 67-77.
16. C. Cheng, J. Shi, Y. Hu and L. Guo, Nanotechnology, 2017, **28**, 164002.
17. L. Zu, X. Cui, Y. Jiang, Z. Hu, H. Lian, Y. Liu, Y. Jin, Y. Li and X. Wang, Materials, 2015, **8**, 1369-1383.
18. M. Aymen, S. Sami, S. Ahmed, G. Fethi and B. M. Abdellatif, J. Phys. D Appl. Phys., 2013, **46**, 335103.
19. A. Rohom, P. Londhe and N. Chaure, Nanosci. Nanotechnol., 2016, **6**, 83-87.
20. A. Bahuguna, P. Choudhary, T. Chhabra and V. Krishnan, ACS omega, 2018, **3**, 12163-12178.